

Electronic Supplementary Information for

### Quinonoid radial $\pi$ -conjugation

Rameswar Bhattacharjee<sup>1\*</sup>, J. D. Tovar<sup>2</sup>, Miklos Kertesz<sup>1\*</sup>

<sup>1</sup>Department of Chemistry, Georgetown University, Washington, D.C. 20057, United States.

<sup>2</sup>Department of Chemistry, and Department of Materials Science and Engineering, Johns Hopkins University, 3400 North Charles Street, Baltimore, MD 21218, United States

#### Table of contents

1. Band gap and bond length information for the [8]C(TPz)<sub>8-x</sub>(PP)<sub>x</sub> and [8]C(ITN)<sub>8-x</sub>(PP)<sub>x</sub> series, Table S1.
2. Comparison of structural parameters with and without D3 dispersion in B3LYP functional, Table S2.
3. Optimized structures, HOMO, LUMO, and band gap ( $E_g$ ) of all the discussed systems, Figures S1-S19, S21-S23, S35-S36.
4. Computed UV-Vis spectra of selected systems, Figures S24-S31.
5. Singlet-triplet energies and gaps, Figure S32.
6. Bond orders, HOMA indices, Figure S33.
7. Energy levels with midgap states, Figure S34.
8. Isomerization data, Figures S37-S39 and Table S3.
9. T1 test results from DLPNO-CCSD(T), Table S4.
10. References.

Table S1. HOMO-LUMO gaps as a function of x together with characteristic 1-1' CC bond distances

<b>[8]C(TPz)<sub>8</sub>- x(PP)<sub>x</sub></b>	E <sub>g</sub> (eV)	1-1' Distance (Å) from TPz to TPz	1-1' Distance (Å) from TPz to PP (next)	1-1' Distance (Å) from PP to PP
Poly(PP)	4.02			1.481
Poly(TPz)	1.51	1.370	-	
<b>x=0</b>	1.97	1.361	-	
<b>1</b>	1.61	1.361	1.386	
<b>2</b>	1.15	1.362	1.396	1.420
<b>3</b>	0.78	1.361	1.404	1.434
<b>4</b>	0.39	1.358	1.417	1.461
<b>5</b>	1.55	1.429	1.461	1.485
<b>6</b>	2.22	1.443	1.463	1.485
<b>7</b>	2.64	-	1.465	1.485
<b>8</b>	3.49	-	-	1.484
<b>[6]C(TPz)<sub>6</sub>- x(PP)<sub>x</sub></b>	E <sub>g</sub> (eV)	1-1' Distance (Å) from TPz to TPz	1-1' Distance (Å) from TPz to PP (next)	1-1' Distance (Å) from PP to PP
<b>x=0</b>	2.44	1.356	-	-
<b>1</b>	2.03	1.356	1.377	-
<b>2</b>	1.56	1.356	1.382	1.404
<b>3</b>	1.22	1.355	1.384	1.411
<b>4</b>	0.91	1.351	1.383	1.415
<b>5</b>	2.47	-	1.469	1.487
<b>6</b>	3.20	-	-	1.487
<b>[8]C(ITN)<sub>8</sub>- x(PP)<sub>x</sub></b>	E <sub>g</sub> (eV)	1-1' Distance (Å) from ITN to ITN	1-1' Distance (Å) from ITN to PP (next)	1-1' Distance (Å) from PP to PP
Poly(PP)	4.02	-	-	1.481
Poly(ITN)	1.64	1.374	-	-
<b>x=0</b>	2.21	1.360	-	-
<b>1</b>	1.77	1.361	1.385	-
<b>2</b>	1.26	1.362	1.392	1.418
<b>3</b>	0.79	1.363	1.402	1.432
<b>4</b>	0.40	1.364	1.414	1.452
<b>5</b>	2.55	1.455	1.466	1.484
<b>6</b>	2.87	1.459	1.468	1.484
<b>7</b>	3.00	-	1.469	1.484

8	3.49	-	-	1.484
---	------	---	---	-------

Table S2: Comparison of optimized structural parameters for three selected  $\pi$ -conjugated macrocycles with and without Grimme's D3 dispersion term in the computation.<sup>a</sup>

System	1-1' Distance (Å)		Diameter (Å)	
	B3LYP-D3/6-311G(d)	B3LYP/6-311G(d)	B3LYP-D3/6-311G(d)	B3LYP/6-311G(d)
[8]CPP	1.484	1.486	10.871	10.888
[8]C(TPz)	1.361	1.361	9.846	9.852
[8]C(ITN)	1.360	1.360	9.922	9.925

<sup>a</sup>Given the small effect on geometry, the effect on the HOMO-LUMO gaps is less than 0.01 eV.

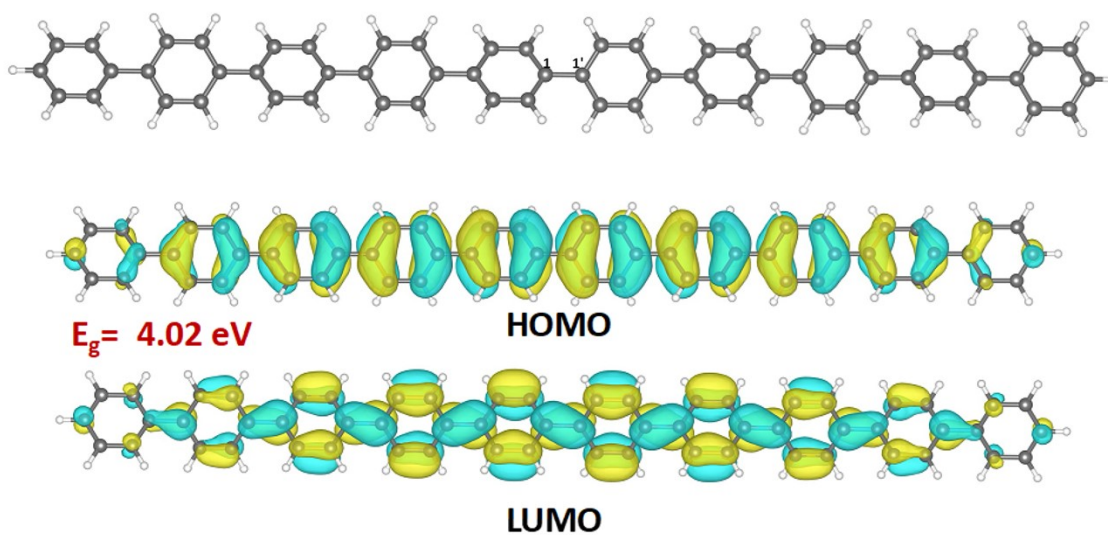


Figure S1: Optimized linear aromatic chain of paraphenylene (PP) containing ten units. HOMO, LUMO and the gap ( $E_g$ ) are also provided.  $D(1-1')=1.481 \text{ Å}$ . The chain is terminated by a hydrogen atom at both ends.

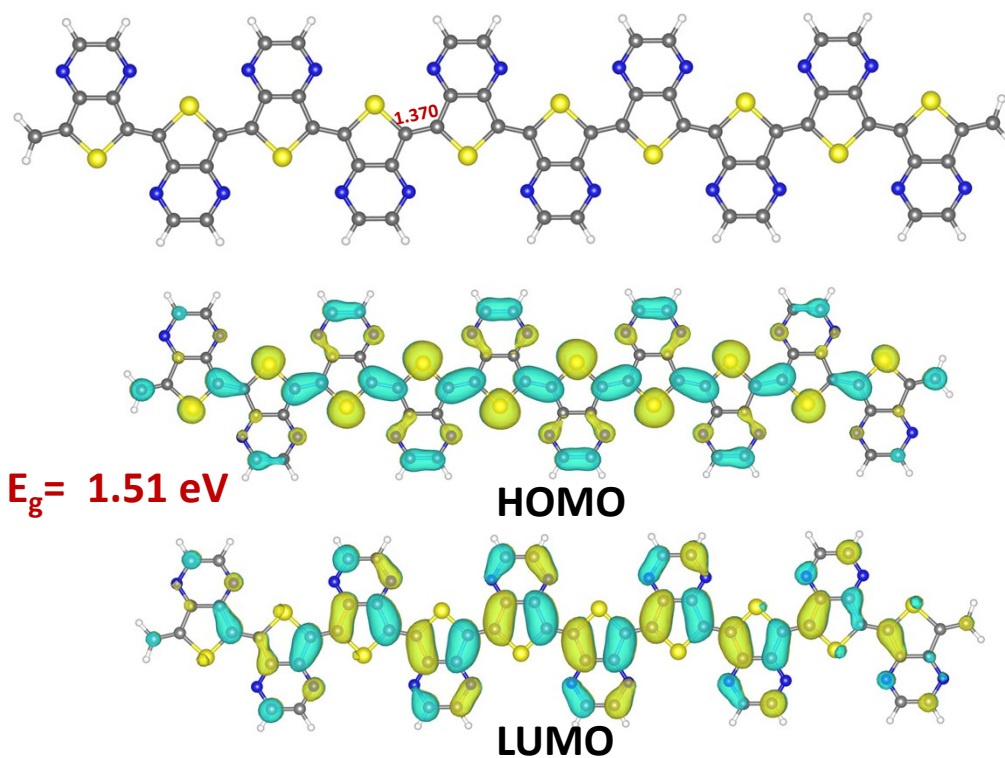


Figure S2: Optimized linear quinonoid chain Thieno[3,4-b]pyrazine, TPz containing ten units. HOMO, LUMO, and the gap ( $E_g$ ) are also provided. The chain is terminated by a  $\text{CH}_2$  group to emphasize the quinonoid structure. The hydrogen atom terminated structure has two localized spins at the termini (edge states, or end states) as discussed in ref.<sup>1</sup>

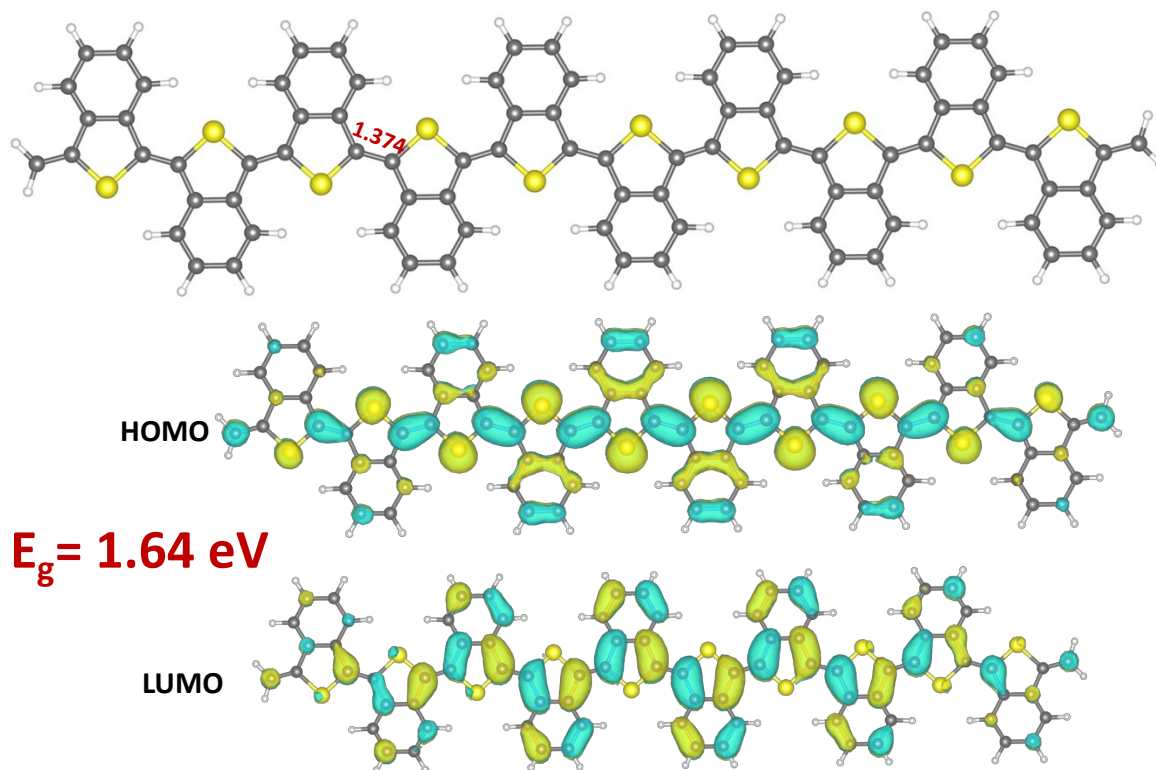


Figure S3: Optimized quinonoid linear chain of Benzo[c]thiophene(isothianaphthene), ITN, along with the corresponding HOMO, LUMO and  $E_g$ . The hydrogen atom terminated structure has two localized spins at the termini (edge states, or end states) as discussed in ref.<sup>1</sup>

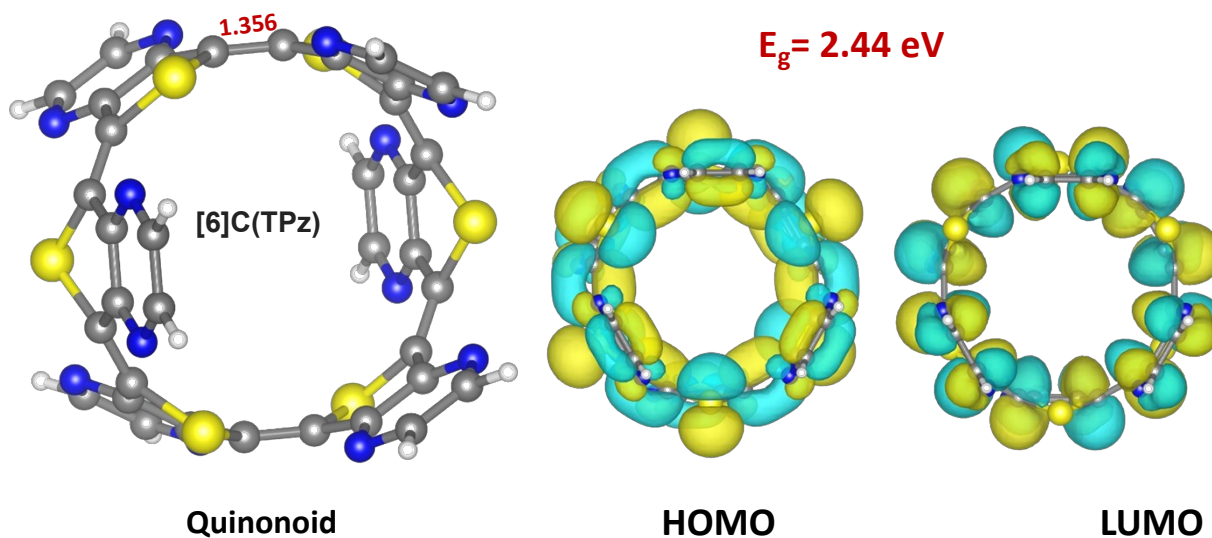


Figure S4: Optimized structure of the cyclic [6]Thieno[3,4-b]pyrazine ([6]C(TPz)) ring, along with the corresponding HOMO, LUMO, and gap ( $E_g$ ).

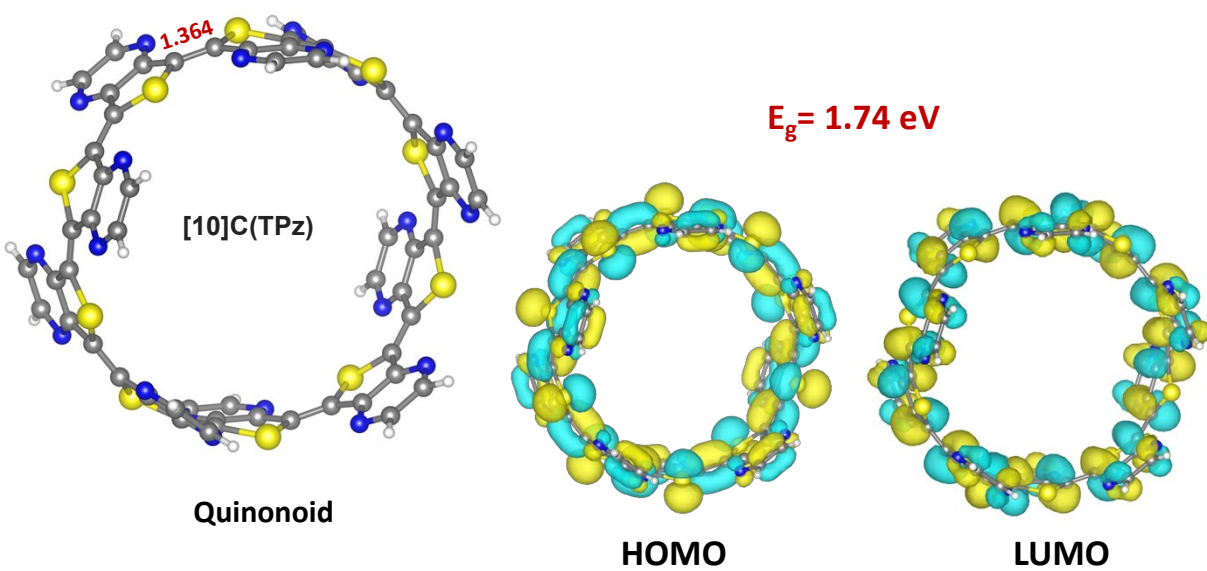


Figure S5: Optimized structure of the cyclic [10]Thieno[3,4-b]pyrazine ([10]C(TPz)) ring, along with the corresponding HOMO, LUMO, and gap ( $E_g$ ).

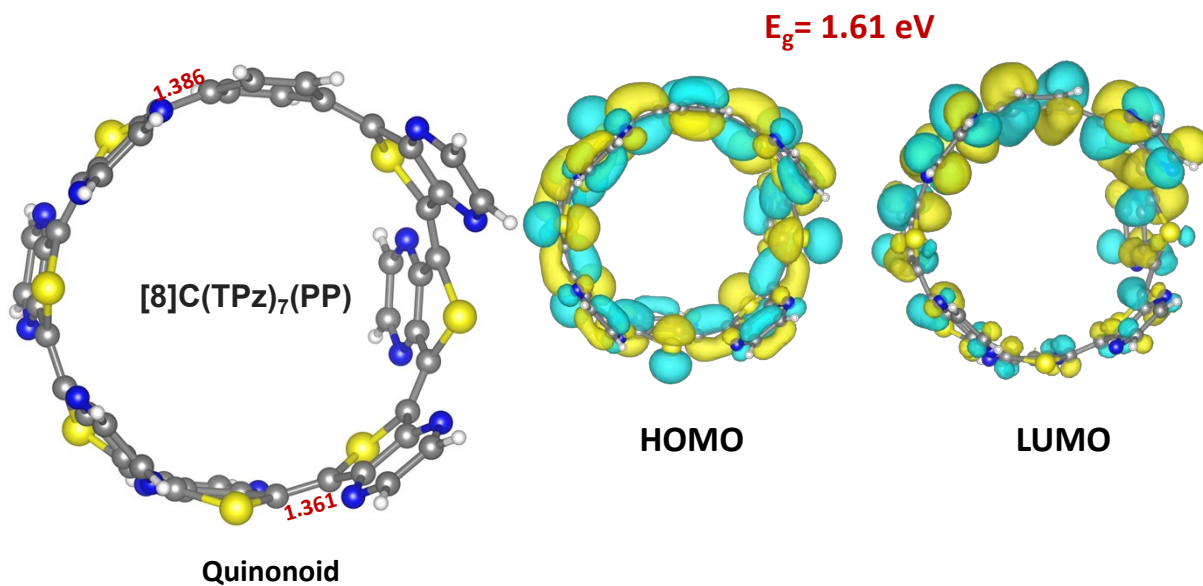


Figure S6: Optimized structure of the cyclic [8]C(TPz)<sub>7</sub>(PP) ring, along with the corresponding HOMO, LUMO, and gap ( $E_g$ ).

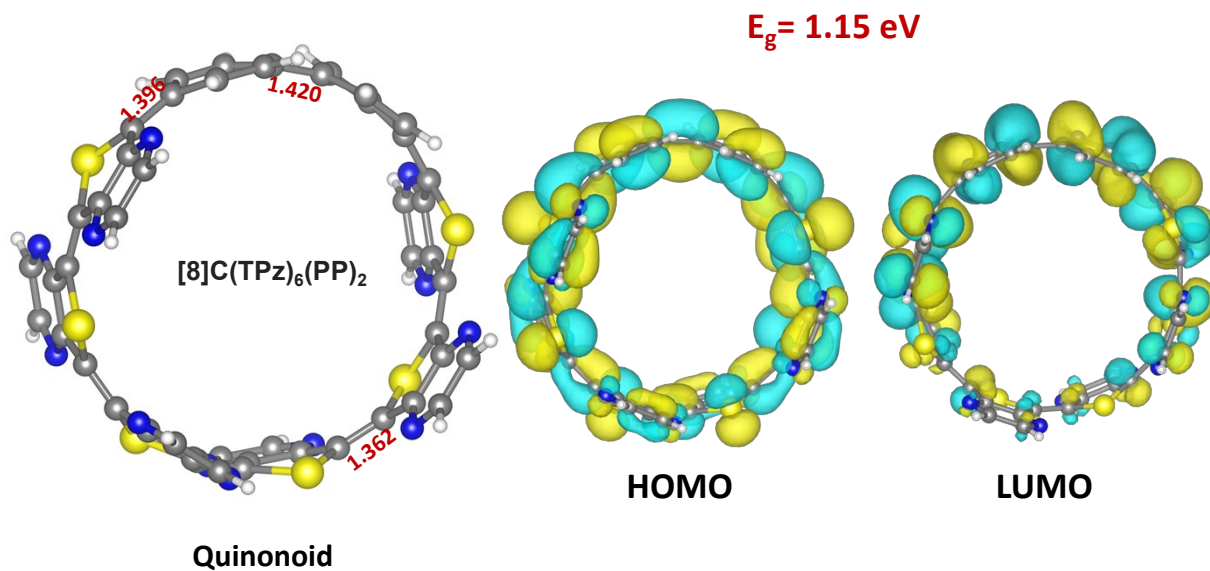


Figure S7: Optimized structure of the cyclic [8]C(TPz)<sub>6</sub>(PP)<sub>2</sub> ring, along with the corresponding HOMO, LUMO, and gap

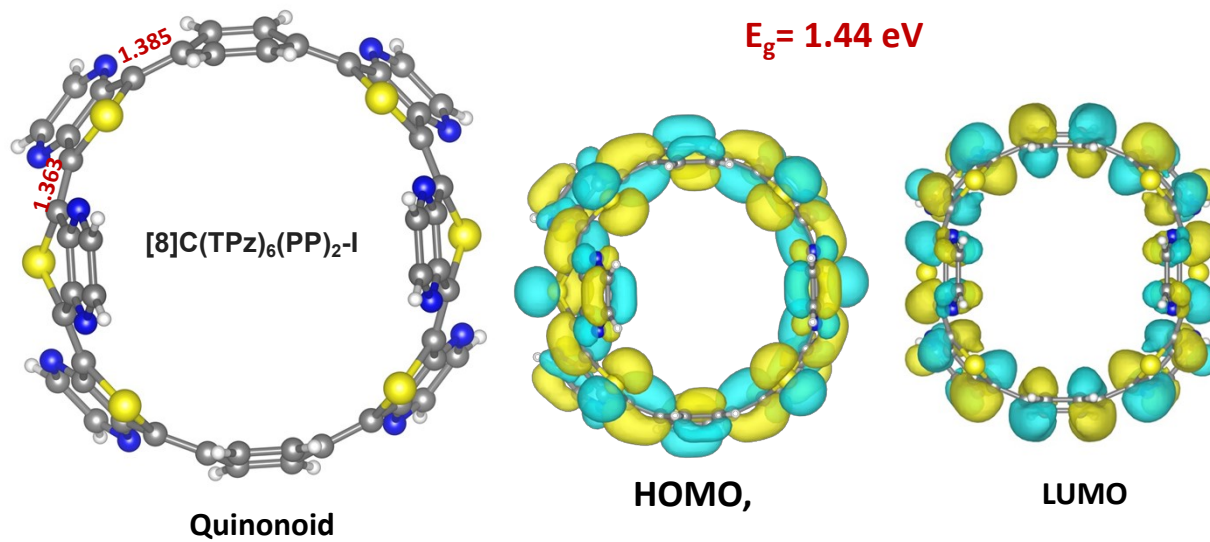


Figure S8: Optimized structure of an alternative configuration of the cyclic [8]C(TPz)<sub>6</sub>(PP)<sub>2</sub> ring, referred to as [8]C(TPz)<sub>6</sub>(PP)<sub>2</sub>-I, along with the corresponding HOMO, LUMO, and gap

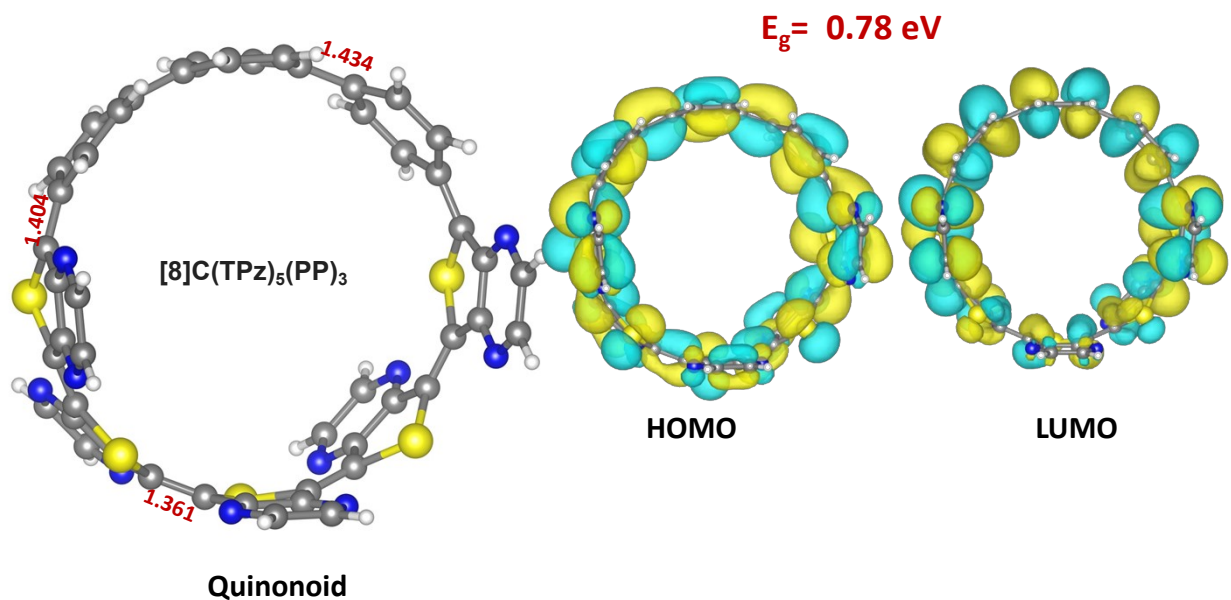


Figure S9: Optimized structure of the cyclic [8]C(TPz)<sub>5</sub>(PP)<sub>3</sub> ring, along with the corresponding HOMO, LUMO, and  $E_g$ .

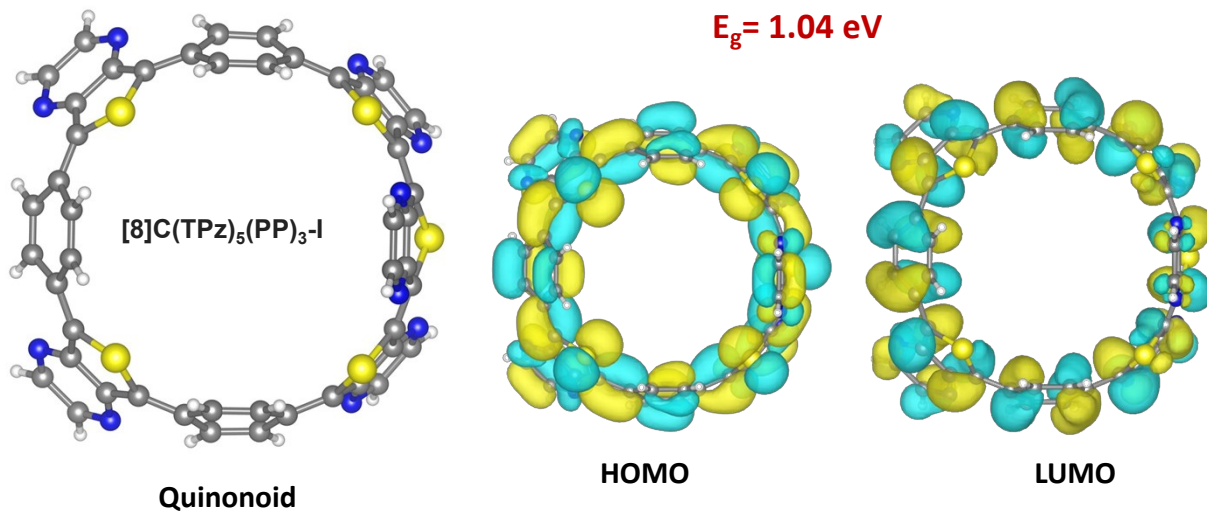


Figure S10: Optimized structure of an alternative configuration of the cyclic [8]C(TPz)<sub>5</sub>(PP)<sub>3</sub> ring, referred to as [8]C(TPz)<sub>5</sub>(PP)<sub>3</sub>-I, along with the corresponding HOMO, LUMO, and gap ( $E_g$ ).

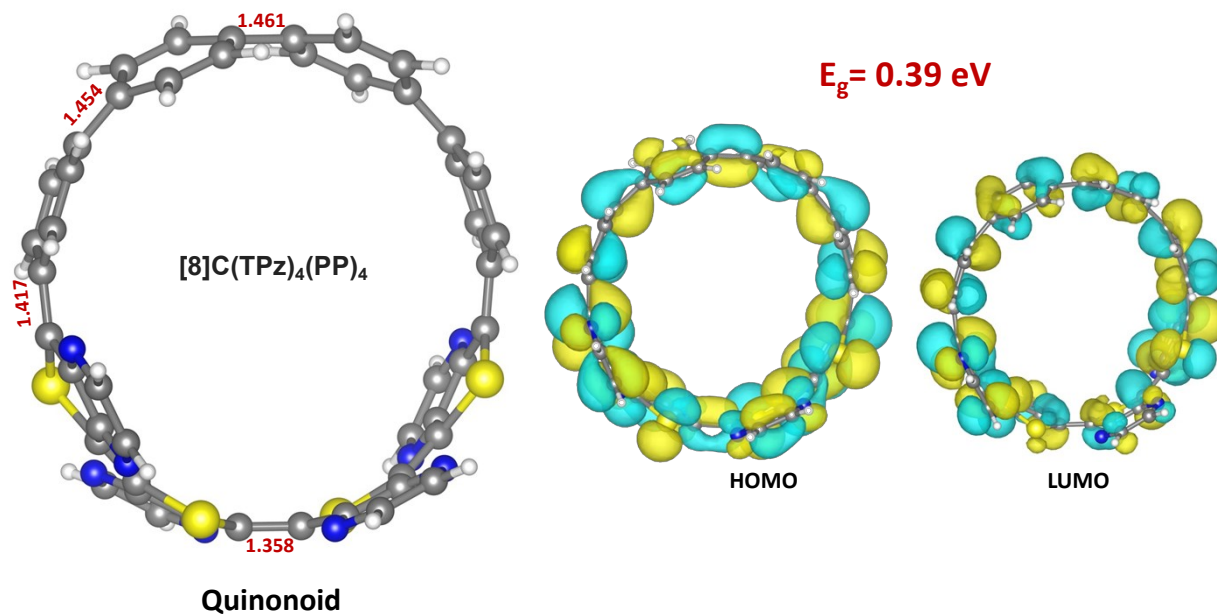


Figure S11: Optimized structure of the cyclic  $[8]C(TPz)_4(PP)_4$  ring, along with the corresponding HOMO, LUMO, and  $E_g$ .

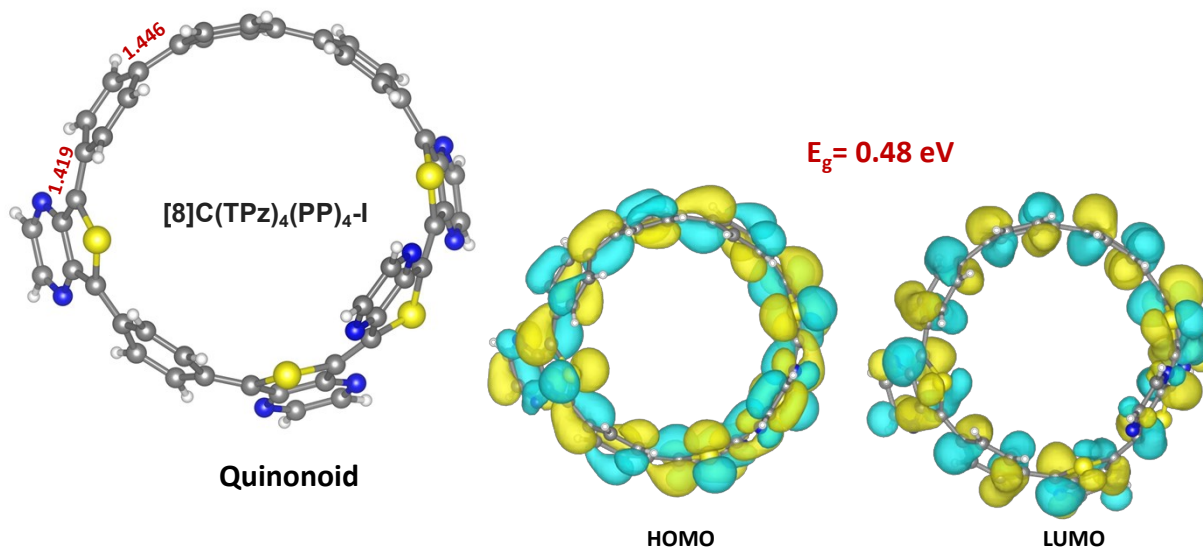


Figure S12: Optimized structure of an alternative configuration of the cyclic  $[8]C(TPz)_4(PP)_4$  ring, referred to as  $[8]C(TPz)_4(PP)_4$ -I, along with the corresponding HOMO, LUMO, and  $E_g$ .

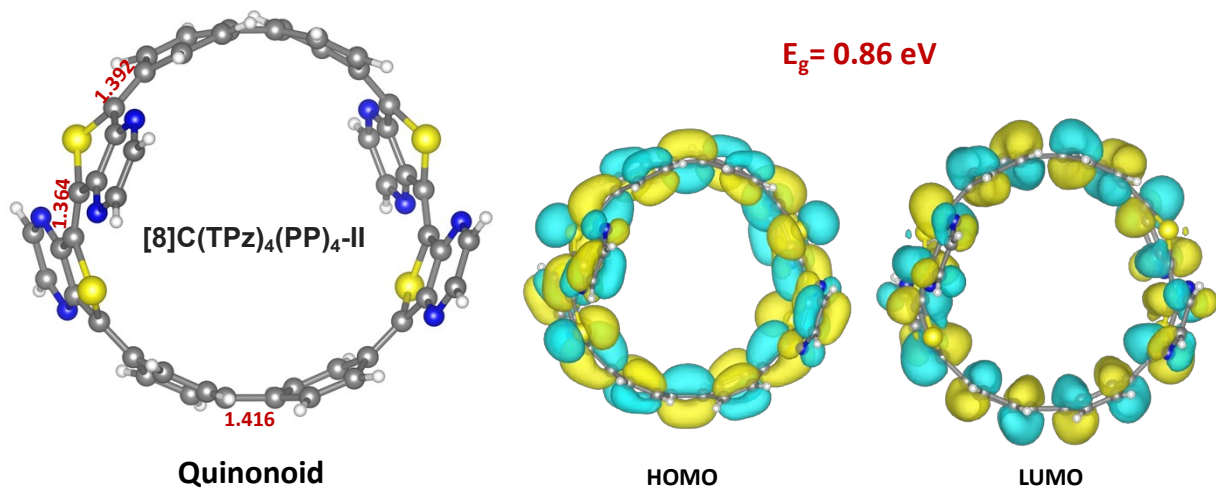


Figure S13: Optimized structure of an alternative configuration of the cyclic [8]C(TPz)<sub>4</sub>(PP)<sub>4</sub> ring, referred to as [8]C(TPz)<sub>4</sub>(PP)<sub>4</sub>-II, along with the corresponding HOMO, LUMO, and  $E_g$ .

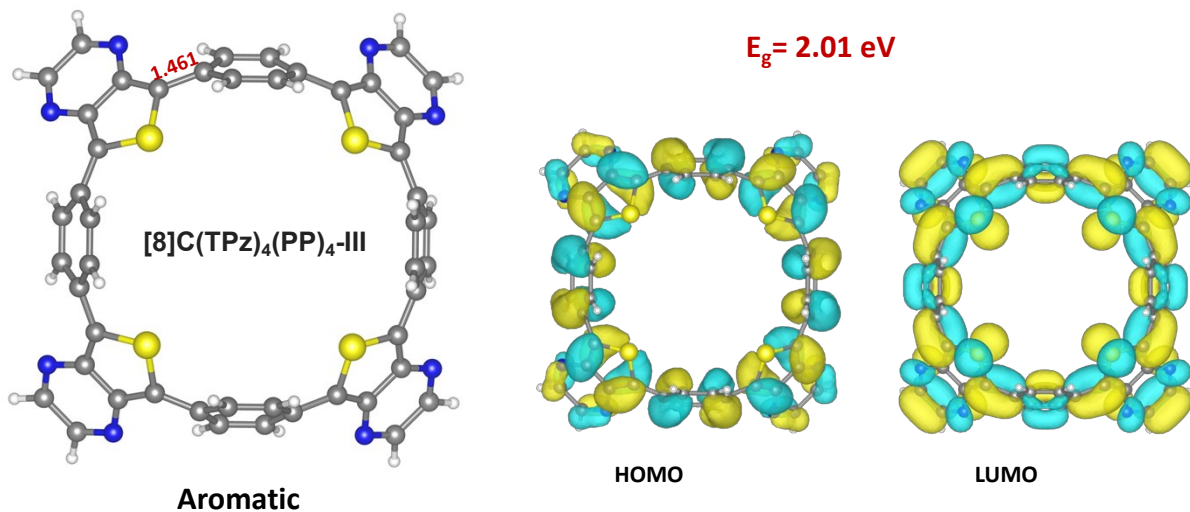


Figure S14: Optimized structure of an alternative configuration of the cyclic [8]C(TPz)<sub>4</sub>(PP)<sub>4</sub> ring, referred to as [8]C(TPz)<sub>4</sub>(PP)<sub>4</sub>-III, along with the corresponding HOMO, LUMO, and  $E_g$ .

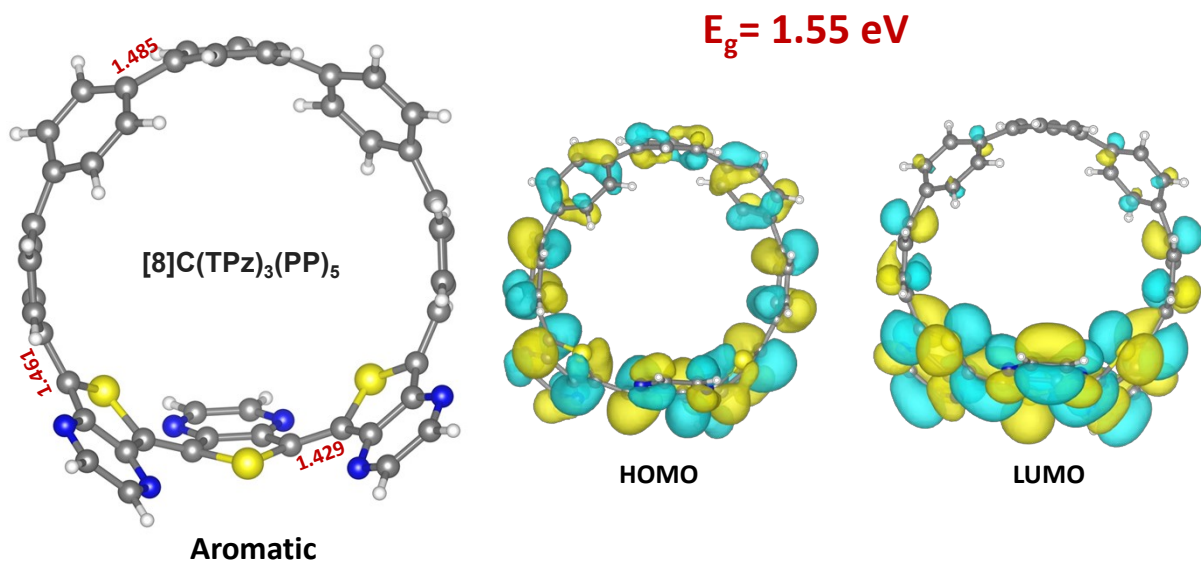


Figure S15: Optimized structure of the cyclic [8]C(TPz)<sub>3</sub>(PP)<sub>5</sub> ring, along with the corresponding HOMO, LUMO, and  $E_g$ .

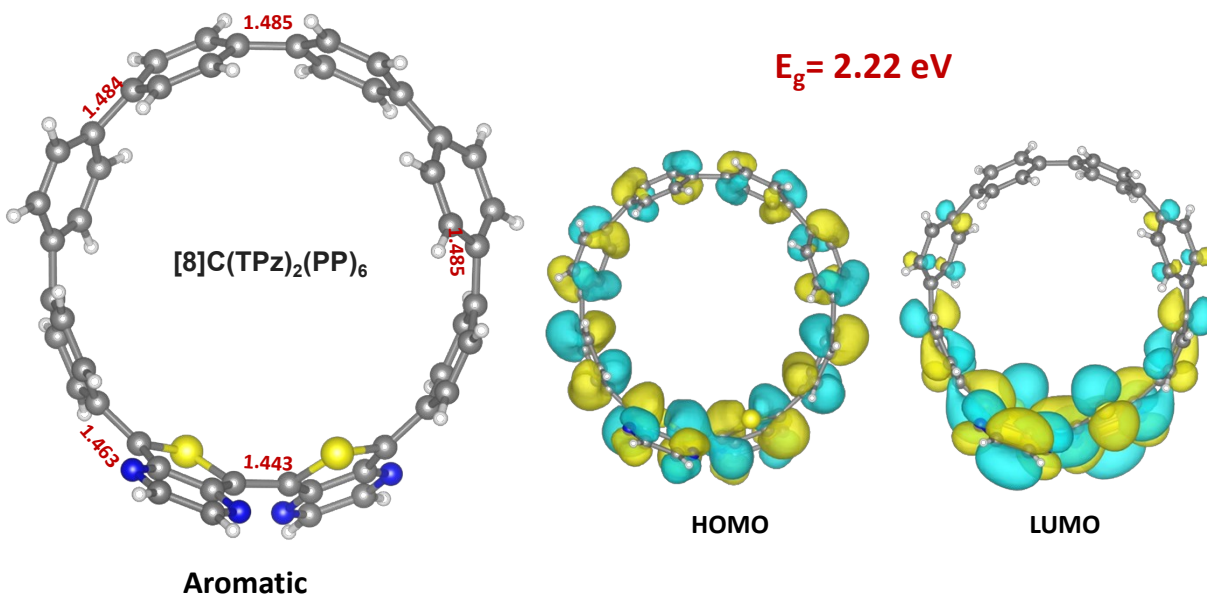


Figure S16: Optimized structure of the cyclic [8]C(TPz)<sub>2</sub>(PP)<sub>6</sub> ring, along with the corresponding HOMO, LUMO, and  $E_g$ .

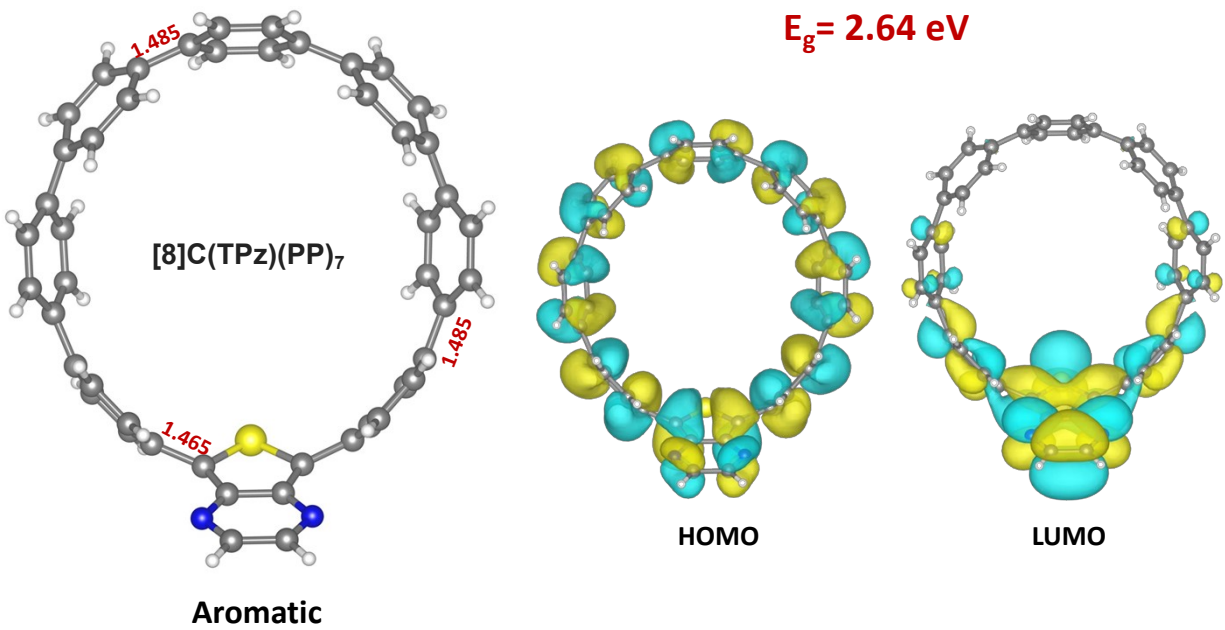


Figure S17: Optimized structure of the cyclic [8]C(TPz)<sub>1</sub>(PP)<sub>7</sub> ring, along with the corresponding HOMO, LUMO, and  $E_g$ .

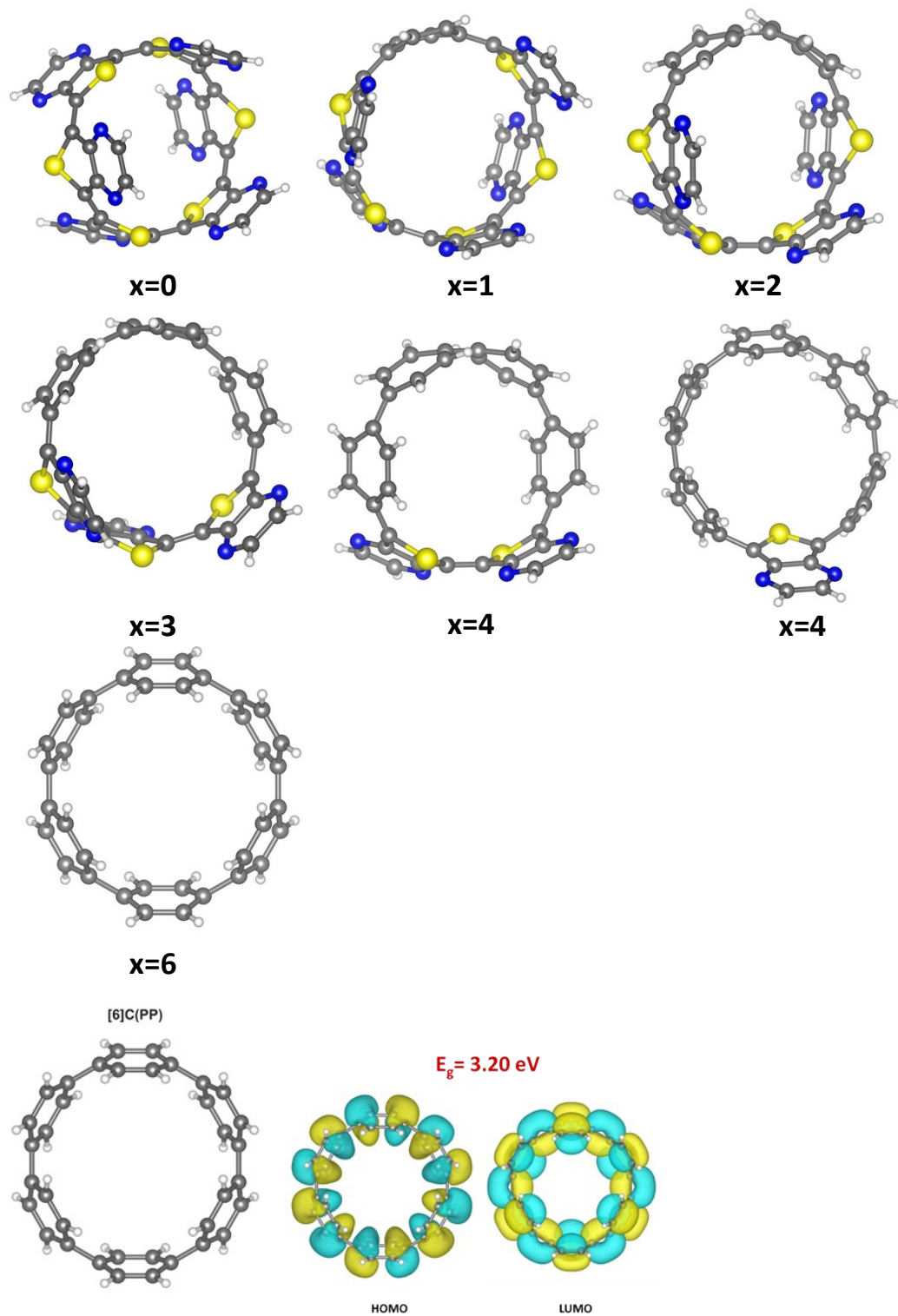


Figure S18: Illustration of selected optimized  $\pi$ -conjugated macrocycles for the  $[6]C(TPz)_{6-x}(PP)_x$  series. Only isomers where the ITN and PP units are not interspersed are shown where they are completely segregated. For  $x=6$  the system is a pure [6]CPP for which the corresponding HOMO, LUMO, and  $E_g$  are also shown.

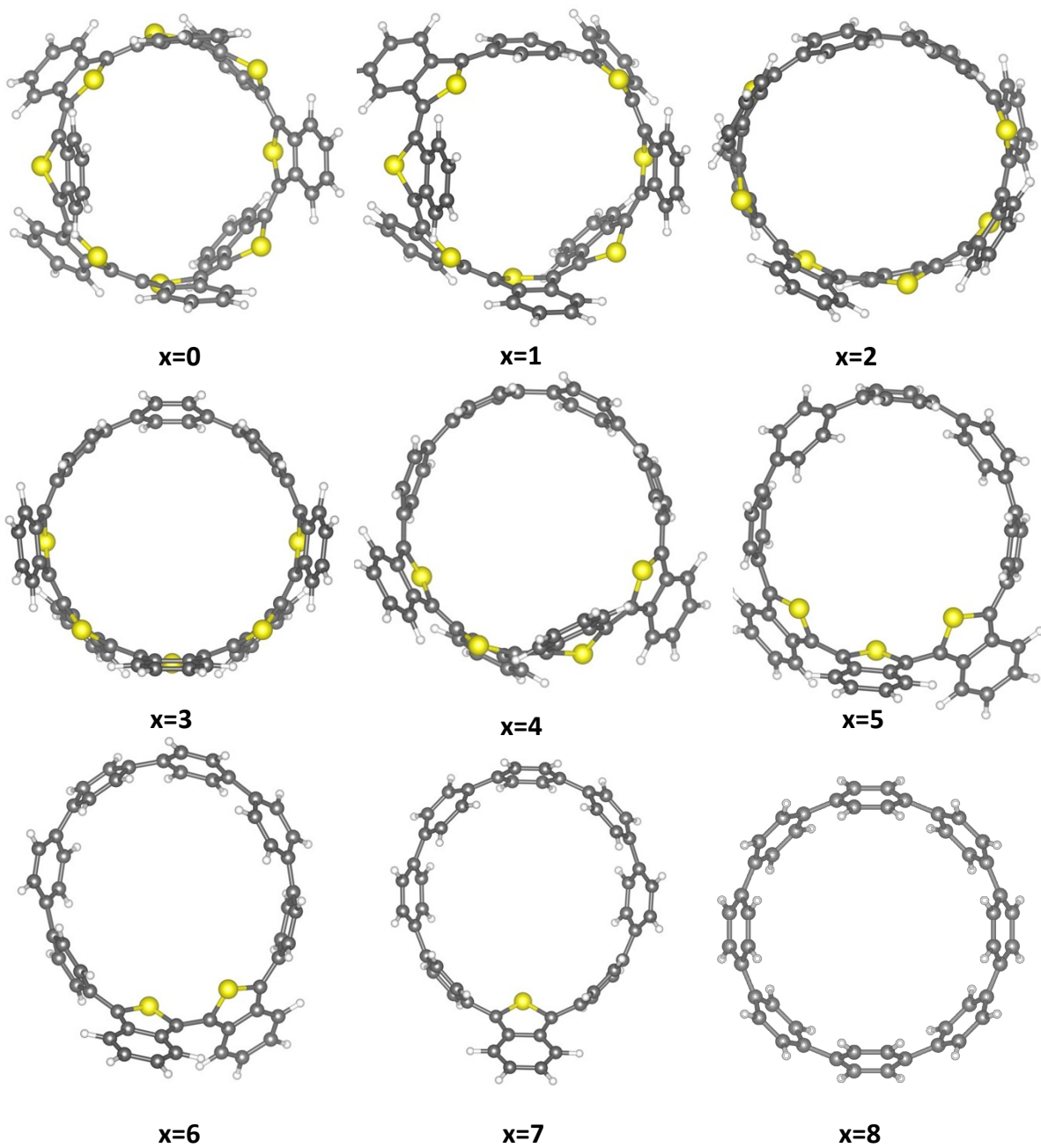


Figure S19: Illustration of selected  $\pi$ -conjugated macrocycles for the  $[8]C(ITN)_{8-x}(PP)_x$ . Only isomers where the ITN and PP units are not interspersed (are completely segregated) are shown. For  $x=8$  the system is a pure  $[8]CPP$ .

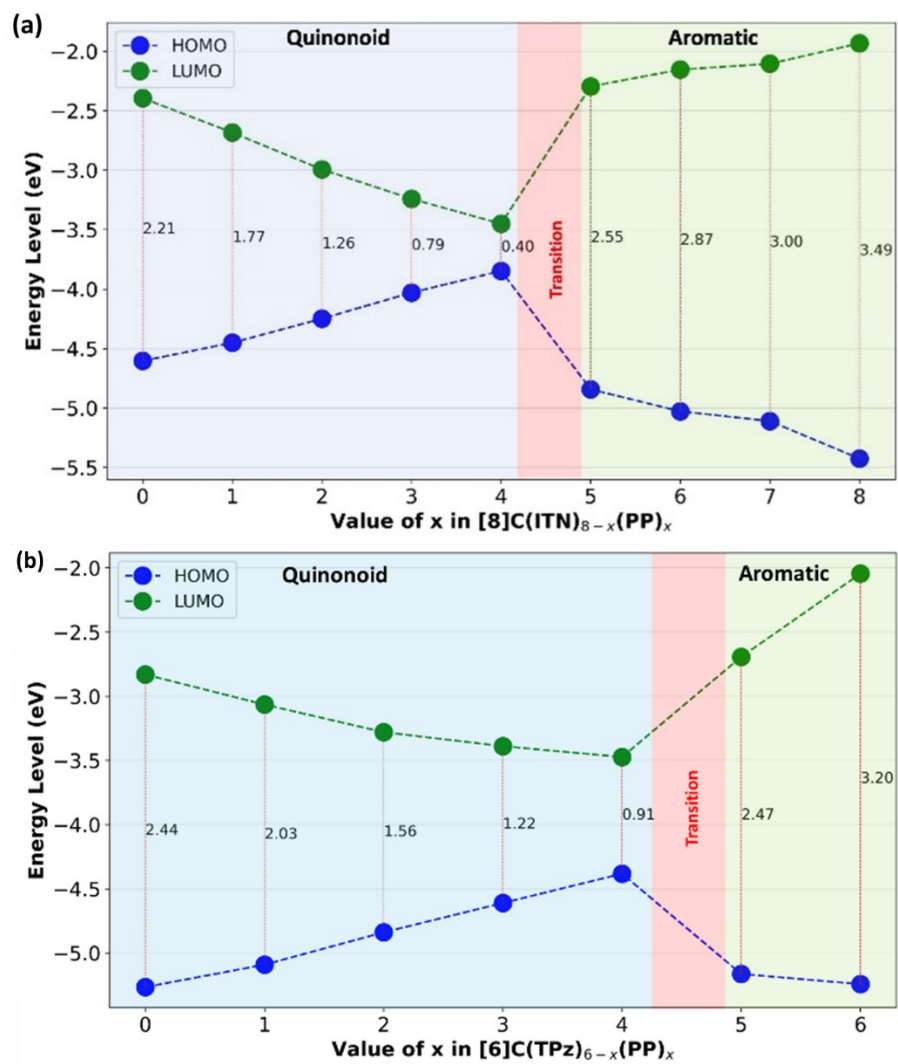


Figure S20. HOMO-LUMO energy gap as a function of  $x$  in the series of  $\pi$ -conjugated macrocycles. (a)  $[8]C(ITN)_{8-x}(PP)_x$ . (b)  $[6]C(TPz)_{6-x}(PP)_x$ . (DFA was B3LYP-D3/6-311G(d).)

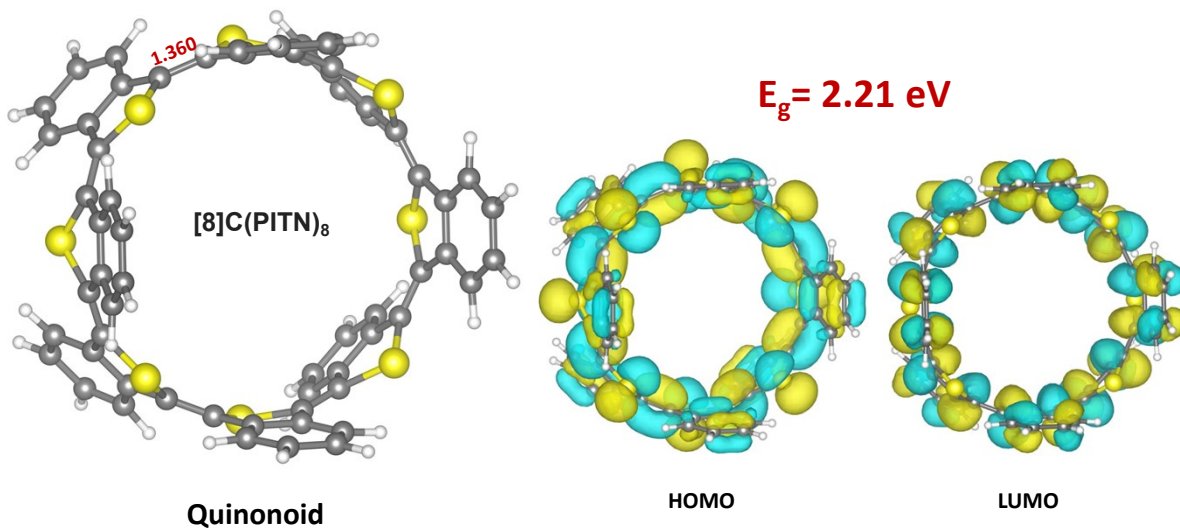


Figure S21: Optimized quinonoid [8]cyclic Benzo[c]thiophene(isothianaphthene), [8]C(ITN), along with the corresponding HOMO, LUMO, and  $E_g$ .

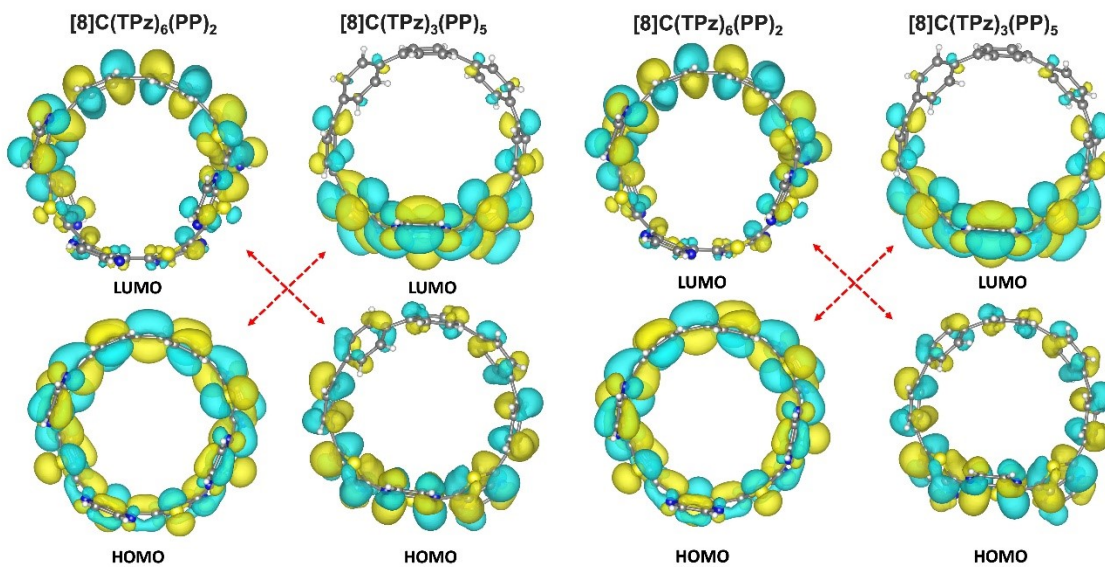


Figure S22: Illustration of orbital level crossing when number of PP unit in the [8]C(PTz)<sub>8-x</sub>(PP)<sub>x</sub> series changes from x=2 to x=5 using two different DFAs: PBE0D3 (left) and M06 (right).

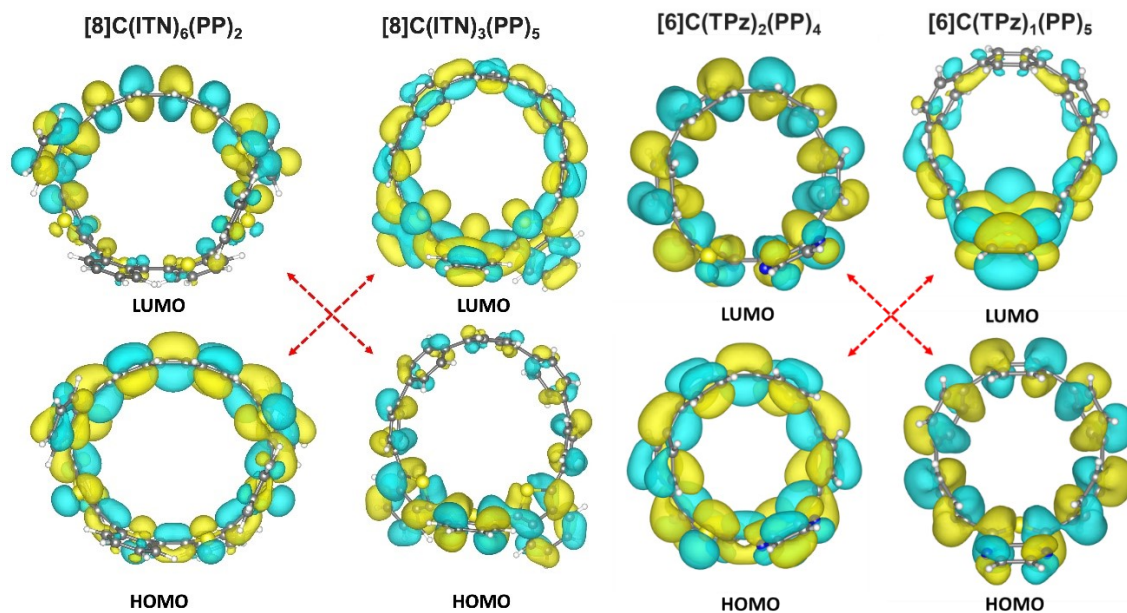


Figure S23: Illustration of orbital level crossing when number of PP unit in the [8]C(ITN)<sub>8-x</sub>(PP)<sub>x</sub> series (left) and in the [6]C(TPz)<sub>6-x</sub>(PP)<sub>x</sub> series, with changes from x=2 to x=5.

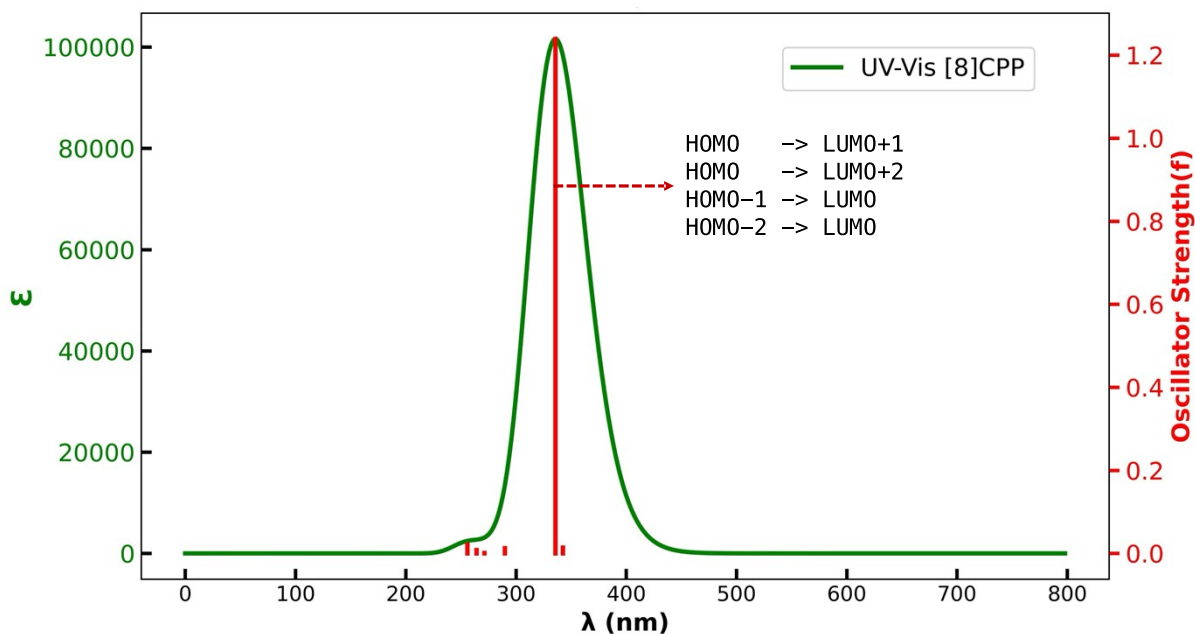


Figure S24: Computed UV-Vis spectra for the [8]CPP, including oscillator strengths, with TDDFT. The excitations corresponding to the highest peak are identified. A default line broadening of 0.333 eV is applied.

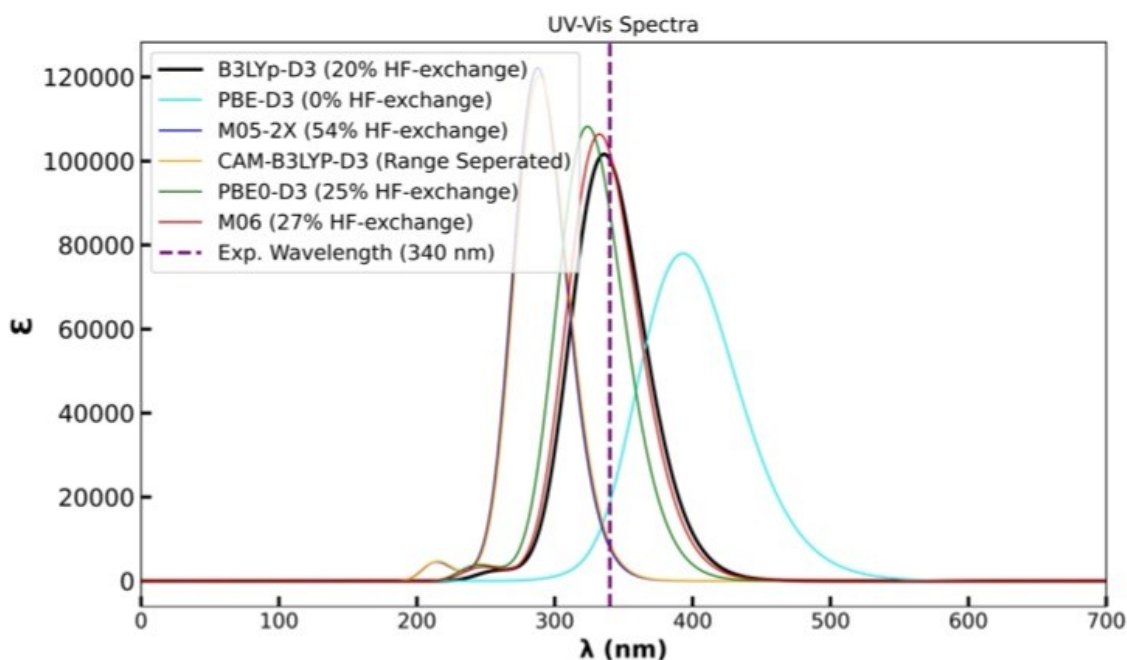


Figure S25: UV-Vis spectra of [8]CPP calculated using various DFT functionals with different amount of HF-exchange. The 6-311G(d) basis set was used. Note, that M05-2X and CAM-B3LYP-D3 overlap completely in this case. The dashed vertical line indicates the experimental value.<sup>2</sup>

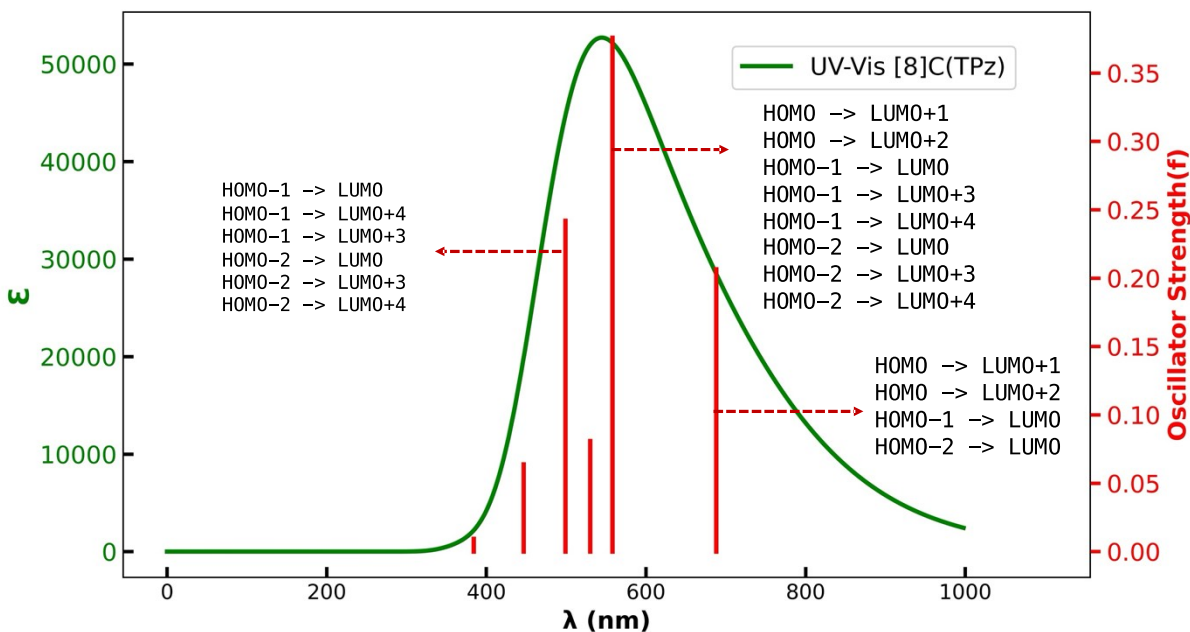


Figure S26. Computed UV-Vis spectra for the [8]C(TPz), including oscillator strengths using TDDFT. The excitations corresponding to the three highest peaks are identified. A default line broadening of 0.333 eV is applied.

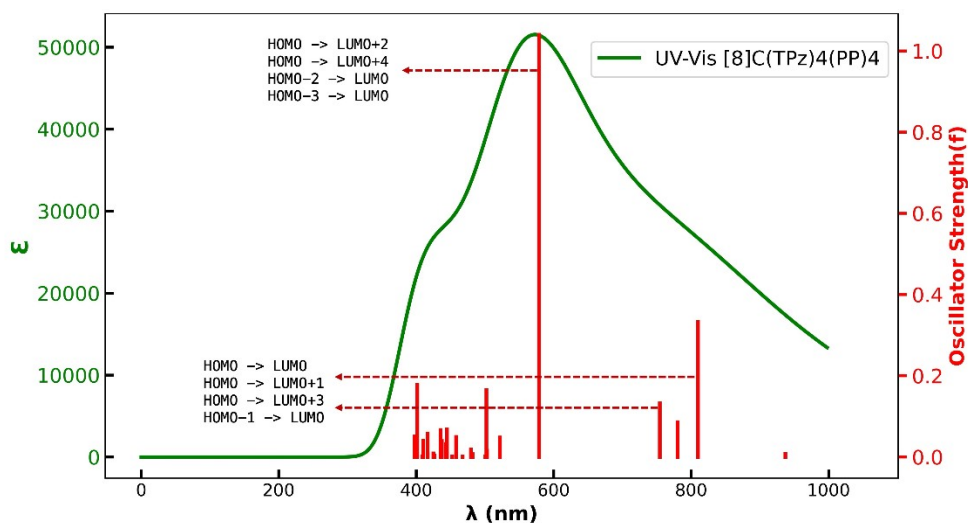


Figure S27: Computed UV-Vis spectra for the  $[8]C(TPz)_4(PP)_4$ , including oscillator strengths using TDDFT. The excitations corresponding to the highest peak is identified. A default line broadening of 0.333 eV is applied.

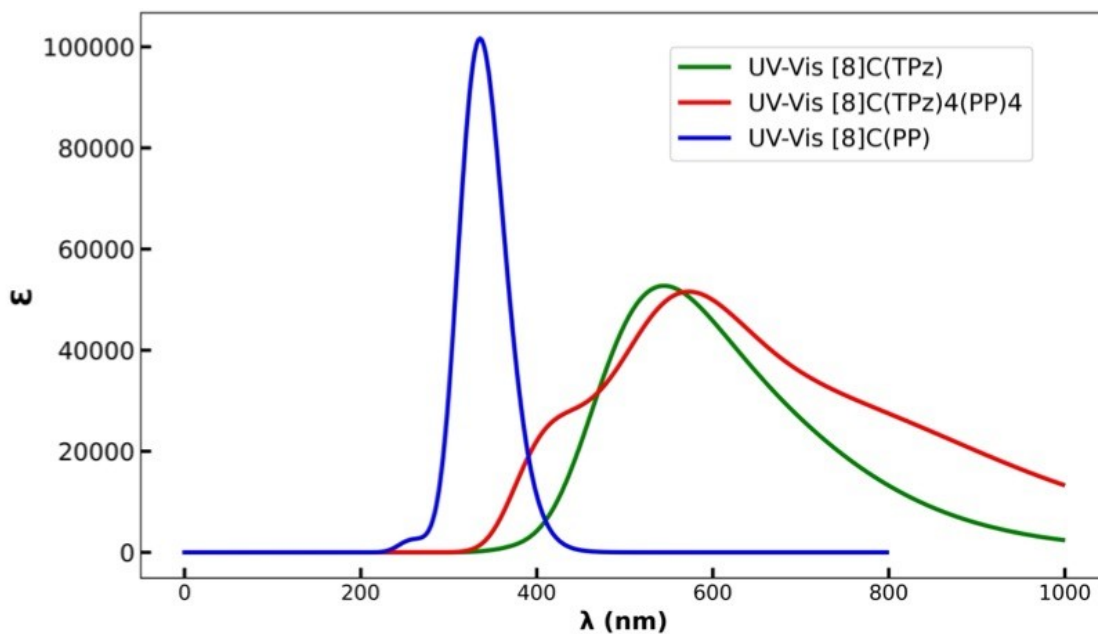


Figure S28: Computed UV-Vis spectra of three macrocycles in the  $[8]C(TPz)_{8-x}(PP)_x$  ( $x=0,4$ , and 8) one plot to understand the shift as the  $x$  value increases.

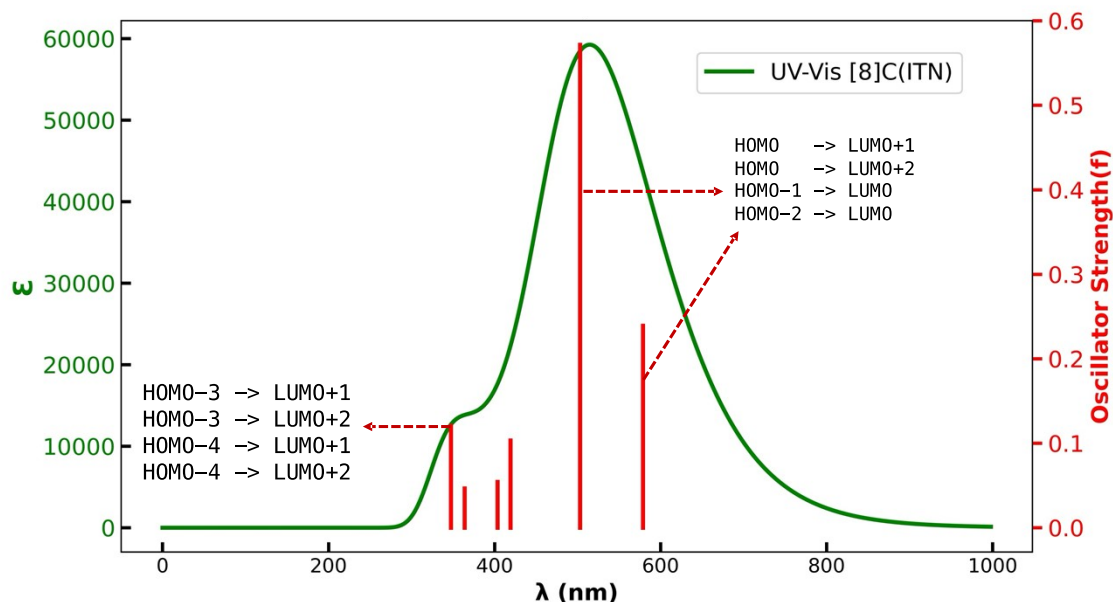


Figure S29: Computed UV-Vis spectra for the [8]C(ITN), including oscillator strengths, using TDDFT. The excitations corresponding to the three highest peaks are identified. A default line broadening of 0.333 eV is applied.

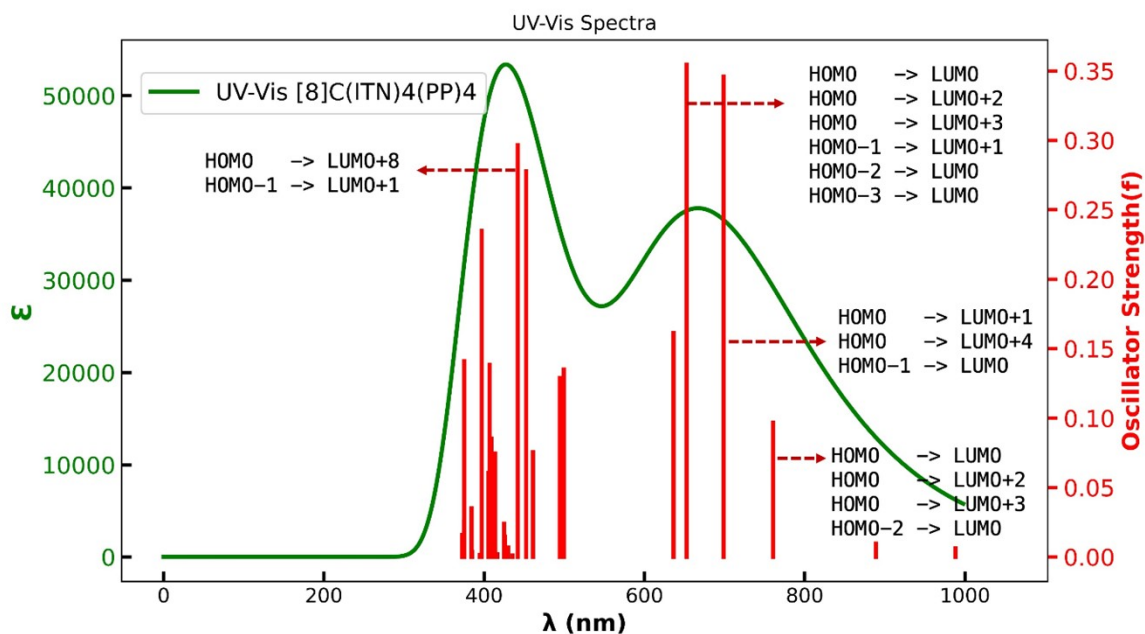


Figure S30: Computed UV-Vis spectra for the [8]C(ITN)<sub>4</sub>(PP)<sub>4</sub>, including oscillator strengths, using TDDFT. The excitations corresponding to the two highest peaks are identified. A default line broadening of 0.333 eV is applied.

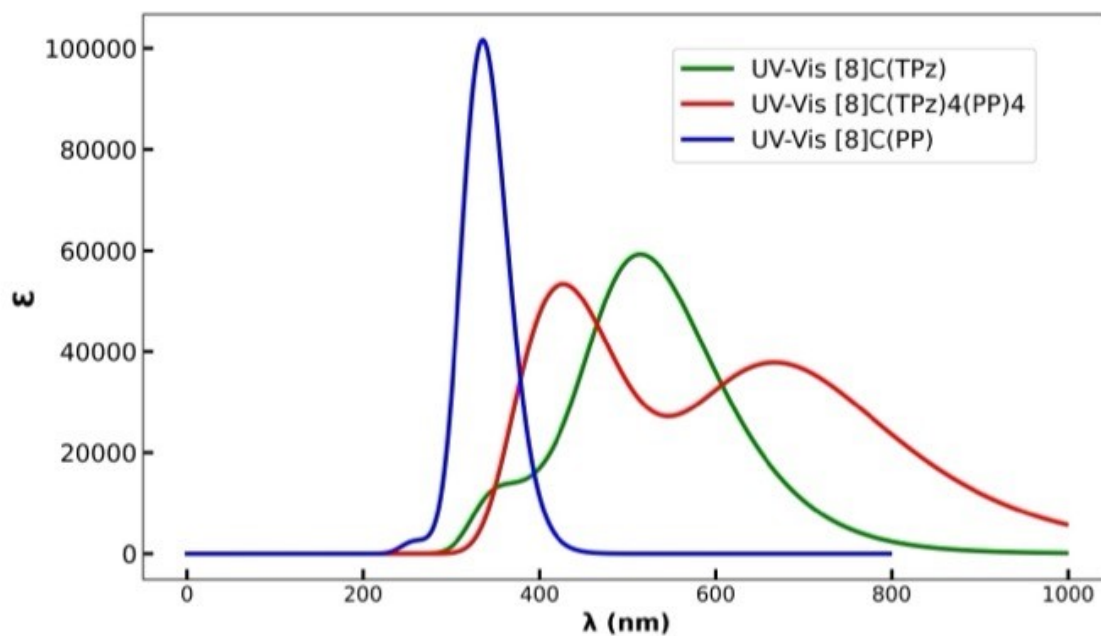


Figure S31. Computed UV-Vis spectra of three macrocycles in the  $[8]C(TPz)_{8-x}(PP)_x$  ( $x=0,4$ , and  $8$ ) series.

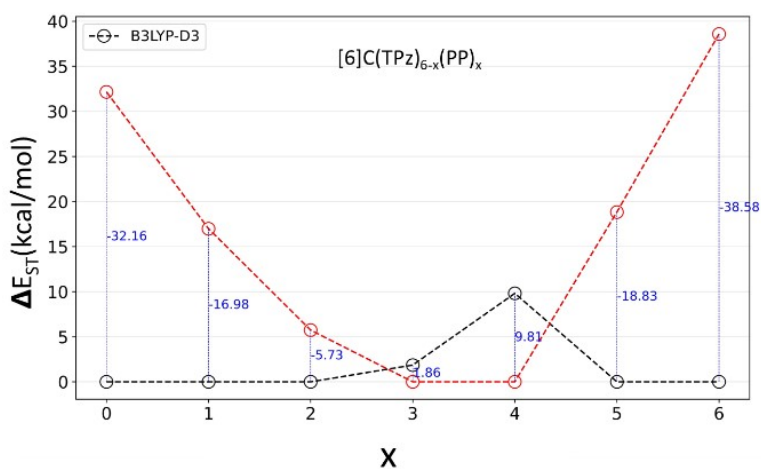


Figure 32. Singlet triplet energy difference,  $\Delta E_{ST}$ , relative to the lower of the two energies, in the  $[6]C(TPz)_{6-x}(PP)_x$  series of mixed nano hoops at the B3LYP-D3/6-311G(d) level. The triplet is more stable for  $x=3$  and  $4$  than the singlet.

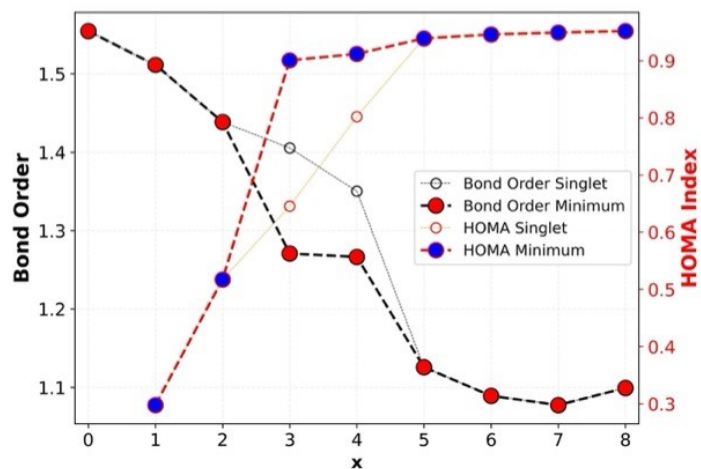


Figure S33: Bond order (left axis) and Harmonic Oscillator Model of Aromaticity (HOMA)<sup>3</sup> index (right axis) as a function of x in cyclic [8]C(TPz)<sub>8-x</sub>(PP)<sub>x</sub> series. The Mayer-Mulliken bond order (from NBO analysis) decreases with increasing benzene content, indicating a loss of extended conjugation. Conversely, the HOMA index rises, suggesting a shift toward localized benzene-like aromaticity.

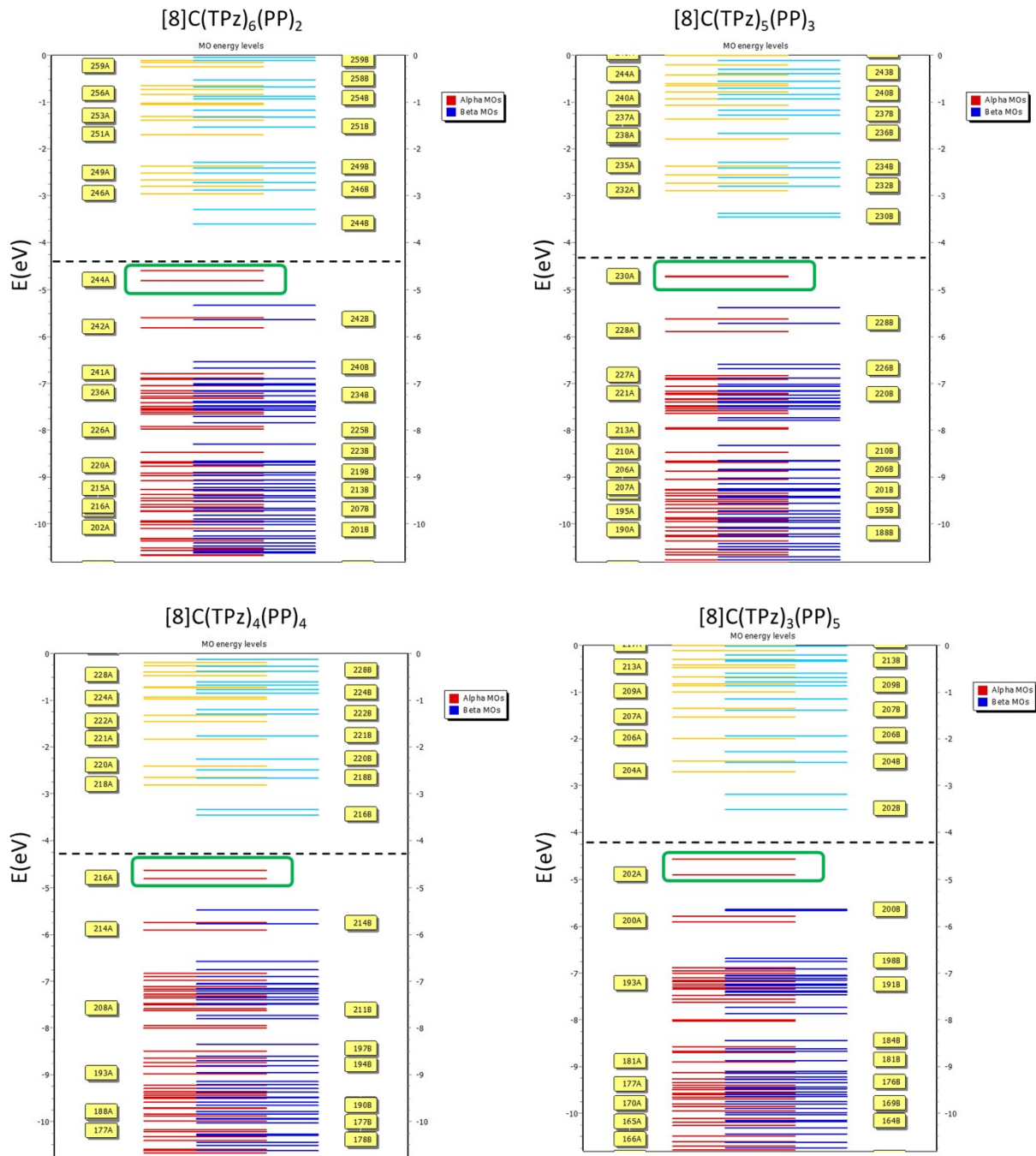


Figure S34: MO energy levels for triplet states of [8]C(TPz)<sub>8-x</sub>(PP)<sub>x</sub> showing the midgap levels indicated by the green boxes. Note that for x=3 the splitting between the two SOMOs in the midgap is only 0.01 eV, and is barely visible in the diagram.

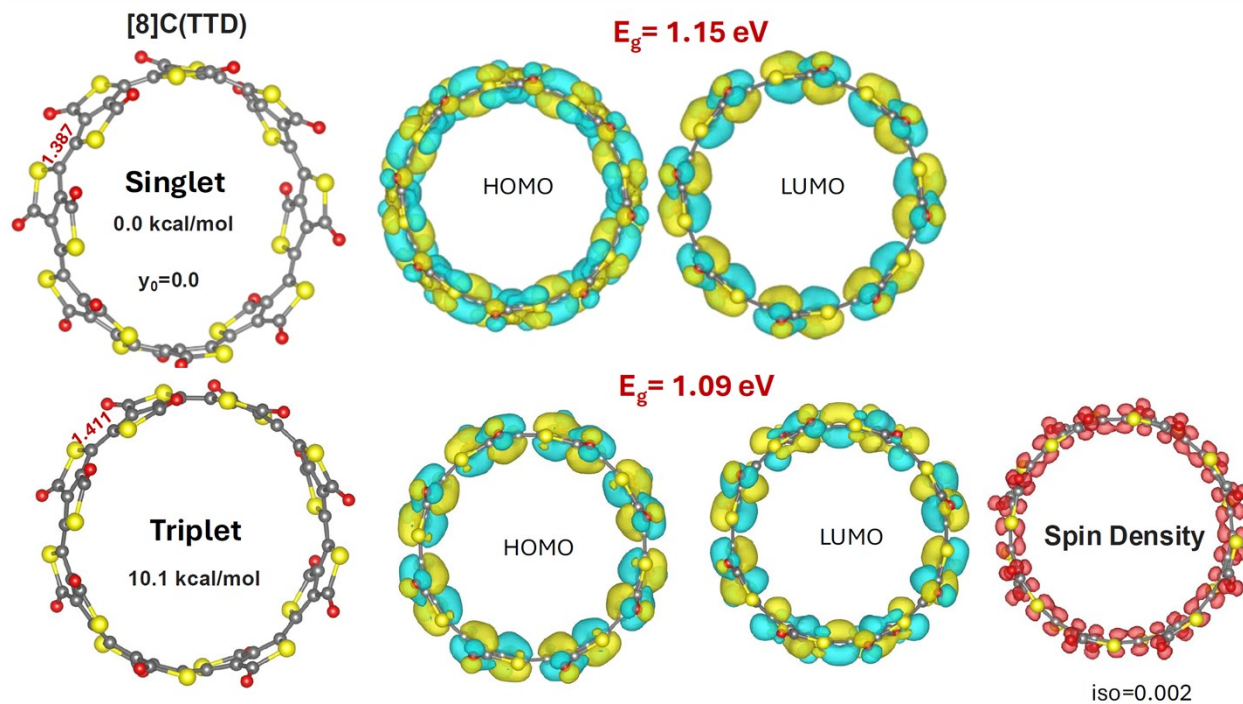


Figure S35: Optimized [8]cyclic-Thieno[3,4-c]thiophene-1,4-dione, [8]C(TTD), along with the corresponding HOMO, LUMO, and  $E_g$ .

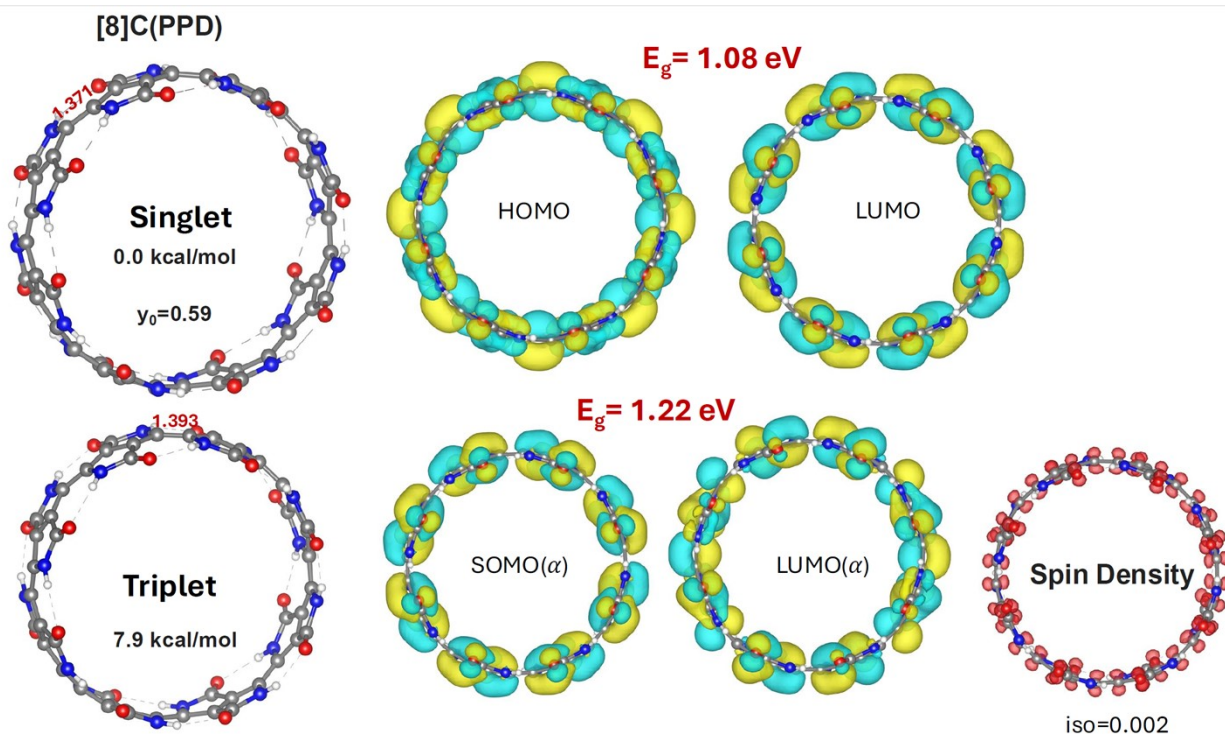


Figure S36: Optimized [8]cyclic-Pyrrolo[3,4-c]pyrrole-1,4-dione, [8]C(PPD), along with the corresponding HOMO, LUMO, and  $E_g$ .

## Isomerization

We first discuss the  $[8]C(TPz)_{8-x}(PP)_x$ . For  $x=1$  and  $7$  there is only one isomer. As  $x$  increases, there are more possibilities to intersperse the aromatic PP units into the otherwise quinonoid ones. For  $x=2$  and  $6$ , there are 4 ways, for  $x=3$  and  $5$ , there are 5 isomers, and finally, for  $x=4$ , there are 8. (for a couple examples, see Figures S37-39 and Table S3). Exploration of the full energetics of this space of a total of 30 isomers is outside the goals of this work. Our focus is finding out if there is an association of the mixing of aromatic and quinonoid units with dramatic changes in their electronic structures.

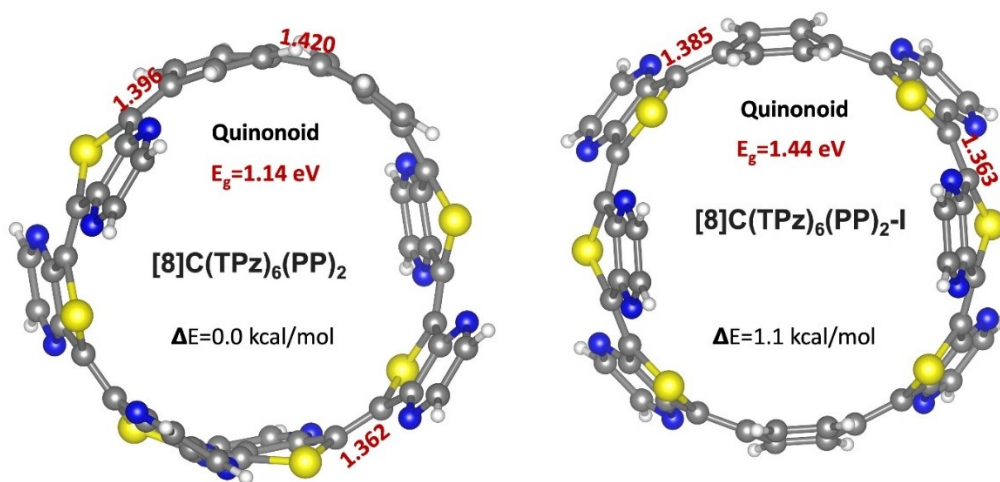


Figure S37: Relative stability of selected two  $[8]C(TPz)_6(PP)_2$  configurations relative to the first configuration where TPz and PP units are maximally segregated.

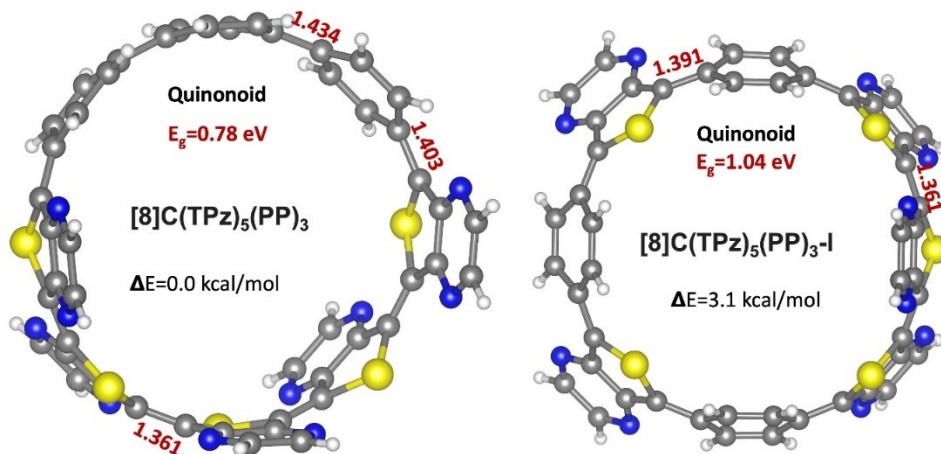


Figure S38: Relative stability of selected two  $[8]C(TPz)_5(PP)_3$  configurations relative to the first configuration where TPz and PP units are maximally segregated.

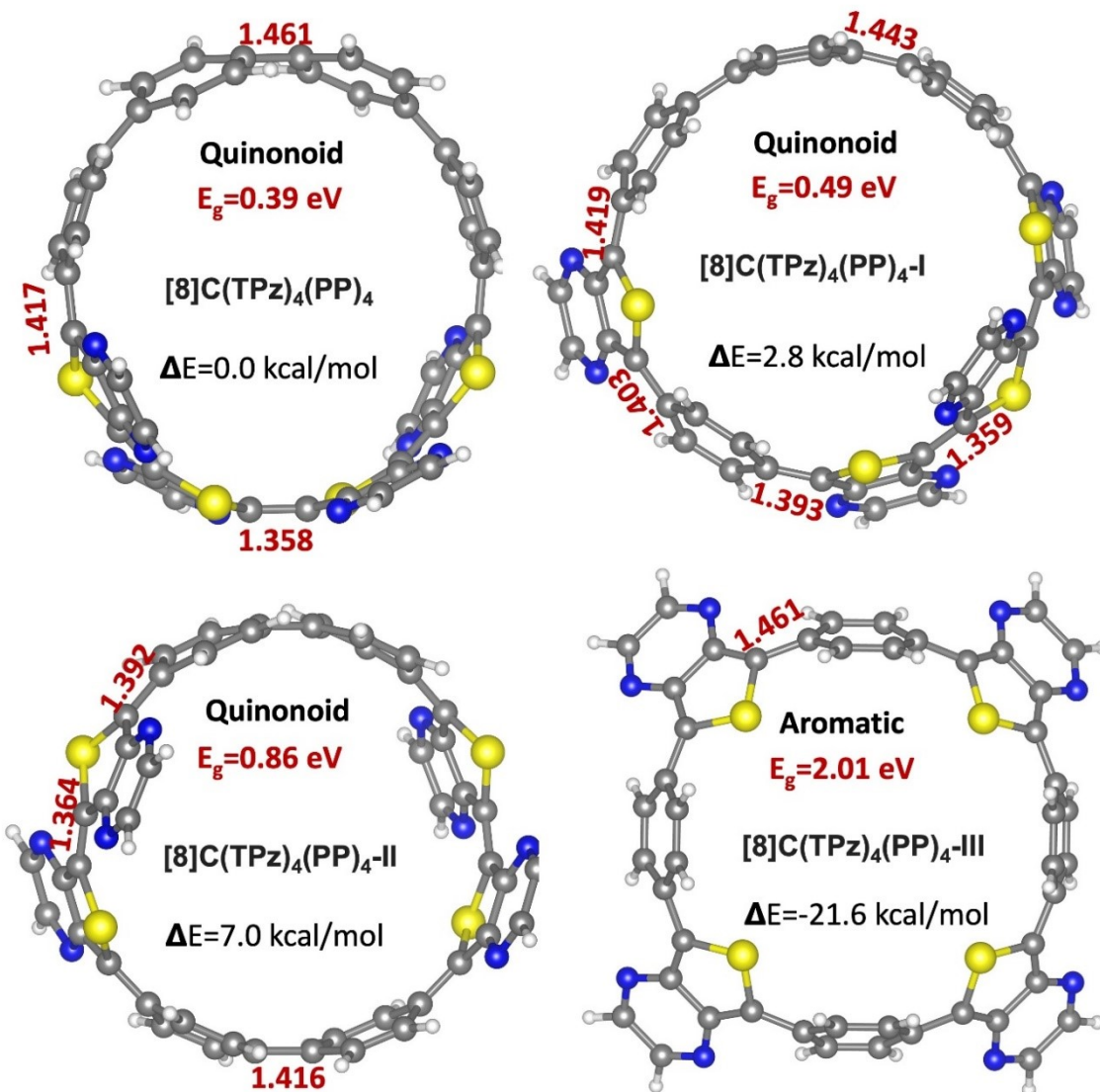


Figure S39: Relative stability of selected  $[8]C(TPz)_4(PP)_4$  configurations relative to the first configuration where TPz and PP units are maximally segregated.

Table S3. Relative stability<sup>a</sup> of selected  $[8]C(TPz)_{8-x}(PP)_x$  isomers (in kcal/mol).

System	Illustrations	Maximally segregated units	I	II	III
$[8]C(TPz)_6(PP)_2$	Figure S37	0	1.1		
$[8]C(TPz)_5(PP)_3$	Figure S38	0	3.1		
$[8]C(TPz)_4(PP)_4$	Figure S39	0	2.8	7.0	-21.6

<sup>a</sup>Relative to the maximally segregated isomer.

Table S4: T1 diagnostic<sup>4</sup> values for the series of [8]C(TPz)<sub>8-x</sub>(PP)<sub>x</sub> (x = 0 to 8), [8]C(TTD), and [8]C(PPD) obtained from DLPNO-CCSD(T)<sup>5</sup>/ def2-SVP// (U)B3LYP-D3/6-311G(d) calculations.

System	Spin State	T1 diagnostic <sup>5</sup>
[8]C(TPz) <sub>8</sub> (PP) <sub>0</sub>	Singlet	0.012051
[8]C(TPz) <sub>7</sub> (PP) <sub>1</sub>	Singlet	0.012048
[8]C(TPz) <sub>6</sub> (PP) <sub>2</sub>	Singlet	0.011942
[8]C(TPz) <sub>5</sub> (PP) <sub>3</sub>	Triplet	0.016444
[8]C(TPz) <sub>4</sub> (PP) <sub>4</sub>	Triplet	0.016408
[8]C(TPz) <sub>3</sub> (PP) <sub>5</sub>	Singlet	0.011713
[8]C(TPz) <sub>2</sub> (PP) <sub>6</sub>	Singlet	0.011142
[8]C(TPz) <sub>1</sub> (PP) <sub>7</sub>	Singlet	0.010648
[8]C(TPz) <sub>0</sub> (PP) <sub>8</sub>	Singlet	0.010157
[8]C(TTD)	Singlet	0.016681
[8]C(PPD)	Singlet	0.015873

## References:

- (1) Cirera, B.; Sánchez-Grande, A.; De la Torre, B.; Santos, J.; Edalatmanesh, S.; Rodríguez-Sánchez, E.; Lauwaet, K.; Mallada, B.; Zbořil, R.; Miranda, R. Tailoring topological order and  $\pi$ -conjugation to engineer quasi-metallic polymers. *Nat. Nanotechnol.* **2020**, *15* (6), 437-443.
- (2) Iwamoto, T.; Watanabe, Y.; Sakamoto, Y.; Suzuki, T.; Yamago, S. Selective and random syntheses of [n] cycloparaphenylenes (n= 8–13) and size dependence of their electronic properties. *J. Am. Chem. Soc.* **2011**, *133* (21), 8354-8361.
- (3) Kruszewski, J.; Krygowski, T. Definition of aromaticity basing on the harmonic oscillator model. *Tetrahedron Lett.* **1972**, *13* (36), 3839-3842.
- (4) Lee, T. J.; Taylor, P. R. A diagnostic for determining the quality of single-reference electron correlation methods. *Int. J. Quantum Chem.* **1989**, *36* (S23), 199-207.
- (5) Riplinger, C.; Pinski, P.; Becker, U.; Valeev, E. F.; Neese, F. Sparse maps—A systematic infrastructure for reduced-scaling electronic structure methods. II. Linear scaling domain based pair natural orbital coupled cluster theory. *J. Chem. Phys.* **2016**, *144* (2).

